JOURNAL OF MATERIALS SCIENCE 24 (1989) 1931–1935

Phase transitions at the crack tip in titanium-modified type 316 stainless steel cathodically hydrogen charged

E. MANOR-MINKOVITZ, D. ELIEZER
Department of Materials Engineering, Ben-Gurion University of the Negev, Beer Sheva, Israel

Phase transitions at the crack tips in solution-annealed titanium-modified (TiM) Type 316 stainless steel resulting from cathodic hydrogen charging in the absence of any externally applied stress, was studied using transmission electron microscopy. The location of the α'-martensite phase was found to occur ahead of the crack tip, in front of the crack, and within the grains of Type 316 TiM after hydrogen charging. Further charging revealed crack propagation through the α'-phase, which strongly suggests the tendency towards transgranular fracture under conditions of high hydrogen fugacities. These results further suggest that the γ-phase stability was not increased as a result of the titanium addition. The possible role of the α'-martensite phase in the fracture mechanism is discussed.

1. Introduction

Austenitic stainless steels are known to transform to α'(bcc) and ε(hcp) martensite phases during plastic deformation at temperatures below the critical M_d temperature (the temperature at which martensite forms from strained austenite) [1–9]. The relative stability of the austenite γ(fcc)-phase is characterized by its tendency to transform to martensite as a result of strain or subzero cooling. The effect of hydrogen on the γ austenite stability is that it decreases the γ-phase stability and thus may induce transformation of the γ-phase to ε and/or α'-martensite phases [10–15], expanded austenite (γ^*) and expanded martensite (ε^*) [8, 16–18] or metastable hydrid phases [19, 20].

Under conditions of high hydrogen fugacities such as cathodic charging [6, 11, 21, 22] or stress corrosion environments [3, 22, 23], transgranular or intergranular low ductility fracture is observed in both "stable" and "unstable" stainless steels. (Stable stainless steels, such as Type 310, and unstable steels, such as Type 304, are relative terms referring to the tendency toward martensitic transformation of the austenite under normal conditions of processing and use of the steels.) However, despite the previous work on the mechanism of hydrogen cracking, the relationship between hydrogen-induced martensite and hydrogen-related fracture has not been established.

Titanium-modified Type 316 stainless steel and other titanium-containing austenitic stainless steels are being considered as candidate materials for near-term fusion devices, and among the critical properties are their strength, ductility and swelling resistance at elevated temperatures. It has been reported that titanium additions markedly decrease the tendency for intergranular fracture upon high-temperature (up to 650° C) creep exposure, which may be caused by titanium combining with nitrogen and sulphur by the Ti(C, N) and $Ti_4C_2S_2$ carbides, respectively [24]. It has also been reported that resistance to swelling of these alloys is improved on the account of the MC particles trapping at their interfaces most of the He generated in the matrix during irradiation [25, 26]. However, besides helium, hydrogen also is produced upon irradiation in the material of the first wall. No transmission electron microscopy (TEM) study of martensitic phase transitions at the crack tip of cathodically hydrogen charged titanium-modified Type 316 stainless steel is available at present.

The purpose of the present investigation was to study in detail by TEM analysis the martensitic phase transitions at the crack tip of titanium-modified (TiM) Type 316 stainless steel resulting from cathodic hydrogen charging in the absence of any externally applied stress.

2. Experimental procedure

Samples of the commercial Type 316 TiM, of the composition shown in Table I, where solution annealed for 1 h at 1100° C and water-quenched. Specimens for TEM were prepared by electrolytic polishing at 65 V in a Tenupol polishing cell using 30 cm^3 perchloric acid, 300 cm^3 methanol and 520 cm^3 butanol solution at −18° C. Because, in the electrolytic polishing process, an attack of the hole edge is normally unavoidable, only prethinned specimens having "perfect" hole edge [7] as shown in Fig. 1a were selected to be suitable for the hydrogen-charging process. After TEM examination to ensure that no deformation of the structure

TABLE I Chemical composition (wt %) of Type 316 TiM stainless steel

Cr	Ni	Mo	Mn	Si	Ti	C	Cu
17.20	10.64	2.09	0.60	0.60	0.21	0.055	< 0.01

0022–2461/89 $03.00 + .12

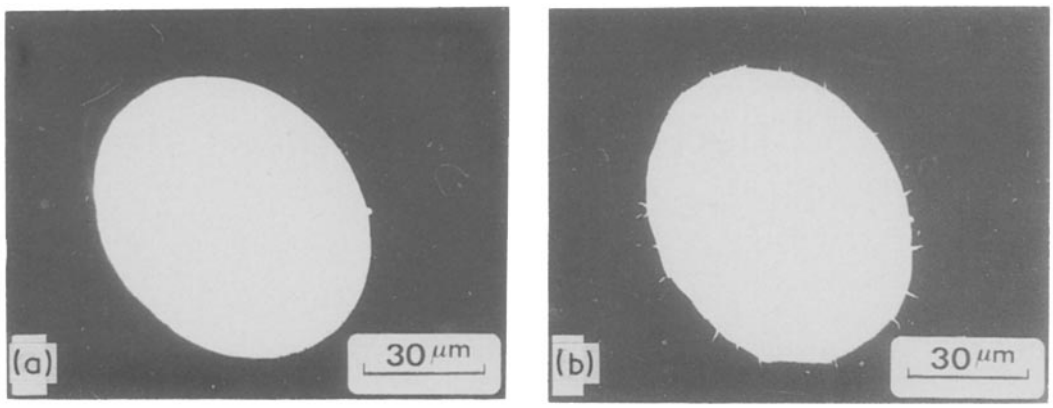

Figure 1 Transmission electron micrographs in the "Mesh-Image" magnification showing the TEM specimen hole of Type 316 TiM stainless steel. (a) "Perfect hole" after the thinning process; (b) cracks which were formed by cathodic charging at the hole edge of the TEM specimen.

had been induced during the thinning process, the specimens were cathodically hydrogen charged and were re-examined by TEM analysis. The cracks usually initiated at the edge of the electropolishing hole and propagated towards the thicker regions of the TEM specimen. The hydrogen charging was performed in a charging cell at room temperature in the absence of any externally applied stress in a 1 N H_2SO_4 solution with 0.25 g $NaAsO_2$ per litre added as hydrogen recombination poison. A platinum counter electrode and a current density of 0.5 A cm^{-2} were used. The charging time was 15 min. The TEM analysis was carried out in a Jeol-200B electron microscope operated at 200 kV.

3. Results and discussion

Transmission electron micrographs taken at the hole edge (shown in Fig. 1a) showing the precipitate size and distribution of the fully annealed Type 316 TiM stainless steel are represented in Figs 2a and b. Selected-area diffraction (SAD) patterns taken from different areas of the TEM specimen revealed that the precipitates were TiC, TiN, and $Ti_4C_2S_2$, where their lattice parameters were very near the values reported in the literature for these phases a_0(TiC) = 0.433 nm [27], a_0(TiN) = 0.424 nm [28], $a_0(Ti_4C_2S_2)$ = 0.312 nm; $c_0(Ti_4C_2S_2)$ = 1.120 nm [29].

Forming cathodic hydrogen charging to the same specimen (shown in Fig. 1a) in the absence of any externally applied stress revealed both intergranular and transgranular cracks at the hole edge (Fig. 1b). Analysis of the phase transitions occurring at the crack tip of one of these transgranular cracks is represented in Figs 3 and 4. The microstructural features around the transgranular crack of the charged specimen are shown in the bright-field electron micrograph (Fig. 3a). SAD patterns taken at the crack tip and its schematic diagram are represented in Figs 4a and b, respectively. These findings revealed single-crystal spot patterns which were indexed as the austenite matrix γ(fcc) and the martensite phase α'(bcc) (Fig. 4b). Fig. 4c represents a superimposed stereogram of the γ-matrix and the α'-martensite with the following γ/α' orientation relationships

γ/α'(NW) (Nishiyama–Wasserman) [30, 31]

$$(1\,1\,1)_\gamma \parallel (0\,1\,1)_{\alpha'}$$

$$[1\,1\,0]_\gamma \parallel [1\,0\,0]_{\alpha'}$$

The patterns of the γ-austenite and α'-martensite reflections are projected on to the stereogram (Fig. 4c) as great circles passing through the points $(3\,\bar{1}\,\bar{1})_\gamma$, $(5\,3\,\bar{1})_\gamma$, $(\bar{1}\,5\,1)_\gamma$, and $(3\,2\,\bar{1})_{\alpha'}$, $(0\,2\,0)_{\alpha'}$, $(\bar{3}\,2\,1)_{\alpha'}$, respectively.

In addition to these phases, the SAD patterns

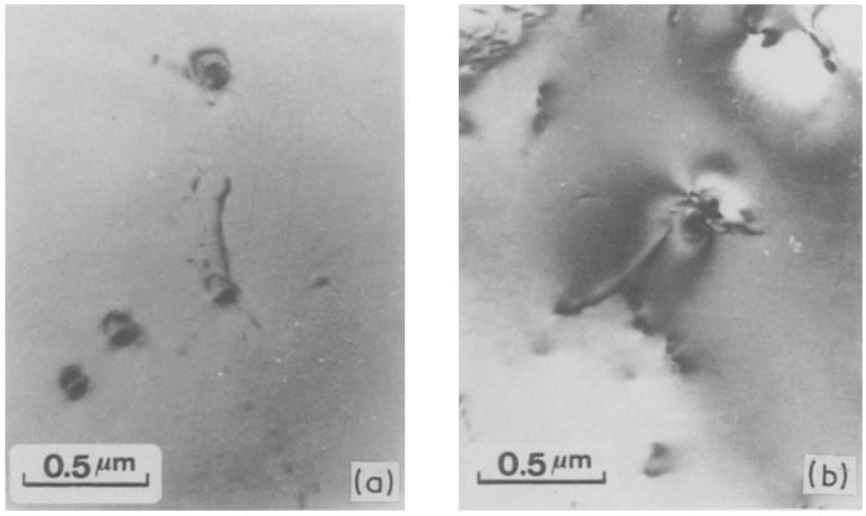

Figure 2 Transmission electron micrographs showing the precipitate size and distribution of the fully annealed Type 316 TiM stainless steel. (a) and (b) Bright-field images taken from different areas of the TEM specimen.

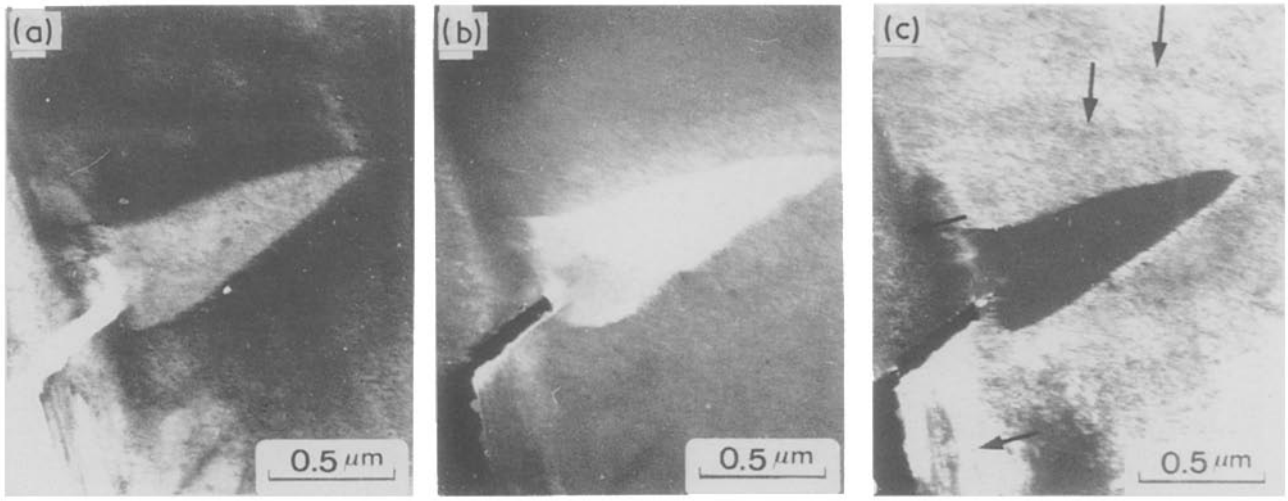

Figure 3 Transmission electron micrographs showing a transgranular crack and the microstructure around the crack of the cathodically hydrogen charged Type 316 TiM stainless steel. (a) Bright-field image; (b) dark-field image, the α'-martensite phase is located in front of the crack; (c) dark-field image, the arrows indicate the presence of the ε-martensite phase.

(shown in Fig. 4a) also revealed additional intensity spots that do not fit either the orientation relationships γ/α' or the $d(h\,k\,l)$ interplanar spacing of both phases. Moreover, on the basis of prior X-ray [16] and TEM [12] information, the expectation in indexing these additional spots in the diffraction pattern was to identify the $\varepsilon(h\,c\,p)$ martensite phase. However, these spots do not fit either the orientation relationships between the γ-austenite matrix and the ε-martensite phase or the interplanar space of the ε-phase. The analysis of such complex diffraction patterns with extra (additional) spots and intensity spikes is described in detail elsewhere [32]. These additional intensity spots appearing in the electron diffraction patterns in several orientations of cathodically hydrogen charged stainless steels were interpreted as arising from $[1\,1\,1]_\gamma$ streaks running through reciprocal lattice points of the ε-martensite phase.

In order to assess the validity of such an interpretation, a special method for determining the exact position of the plane of the diffraction pattern was developed [32]. Thus, using this method it was possible to conclude that the origin of these intensity spots (shown in Fig. 4a and schematically described in Fig. 4b), was very thin hydrogen-induced ε-martensite plates (indicated by arrows in Fig. 3c). The thickness of the ε-phase plates was estimated to be less than 2 nm [32]. The schematic diagram (Fig. 4b) and superimposed stereographic projection (Fig. 4c) of the γ-matrix and the ε-martensite phase with the following γ/ε orientation relationships [33, 34]

$$(1\,1\,1)_\gamma \parallel (0\,0\,0\,2)_{\varepsilon'}$$

$$[0\,1\,\bar{1}]_\gamma \parallel [1\,1\,\bar{2}\,0]_{\varepsilon'}$$

describe the analysis of the SAD pattern of the ε-martensite reflections which appeared as additional intensity spots in Fig. 4a. The nearest great circle to the matrix reflections, corresponding to the low index planes of the ε-phase is projected on to the stereogram (Fig. 4c). These ε-planes $((1\,\bar{1}\,0\,0)_\varepsilon$, $(1\,0\,\bar{1}\,1)_\varepsilon$ and $(0\,1\,\bar{1}\,1)_\varepsilon)$ do not generate diffraction spots, but they are associated with the $[1\,1\,1]_\gamma$ reciprocal lattice streaks, which give rise to observed intensity spots labelled $(1\,\bar{1}\,0\,0)^{st}_\varepsilon$, $(1\,0\,\bar{1}\,1)^{st}_\varepsilon$ and $(0\,1\,\bar{1}\,1)^{st}_\varepsilon$, respectively. (The superscripts st indicate reciprocal lattice streaks and describe the presence of the additional intensity spots in the SAD pattern.) The construction of the diffraction pattern plane by this method (described elsewhere [32]) resulted in a great circle (broken line in Fig 4c) which lies very close to the zone of the matrix reflections. This fact determines that the intensity spots in Fig. 4a are due to the $[1\,1\,1]_\gamma$ streaks running through reciprocal lattice points of the ε-phase.

The ε-martensite plates are located around the crack within the grains of the γ-matrix, as shown in the dark-field image (Fig. 3c) using the $(1\,1\,0\,0)^{st}_\varepsilon$ streak spot.

The dark-field image (Fig. 3b) using the $(0\,2\,0)_{\alpha'}$ reflection showed that the α'-martensite phase is located ahead of the crack tip and in front of the crack. The appearance of the α'-martensite phase was also found within the grains in other regions of the specimen. Further charging to the same specimen and re-examination by TEM studies, revealed crack propagation through the α'-martensite phase.

Transformation of the $\gamma(f\,c\,c)$ phase to $\alpha'(b\,c\,c)$ phase in front of the crack has been shown to occur in "unstable" Type 304, fractured in 10^4 Pa H_2 gas [10] or when Type 304L was cathodically hydrogen charged in the absence of any externally applied stress [11], where the fracture occurred through the α'-phase. In contrast to these findings, crack propagation of Type 304 specimens which were severely embrittled by hydrogen pre-charging and then fractured in air has been shown to occur mainly along the ε-martensite phase and partly in the region having a mixed structure of α' and ε martensite phases [15]. In Type 316L of intermediate γ stability, it has been shown [7] that the γ to ε phase transition occurred in front of the crack. The crack propagated mainly through the ε-phase, while a mixed area of α' within the ε-phase plates could be found ahead of the crack tip. In the more highly alloyed "stable" Type 310, no evidence of

(b)

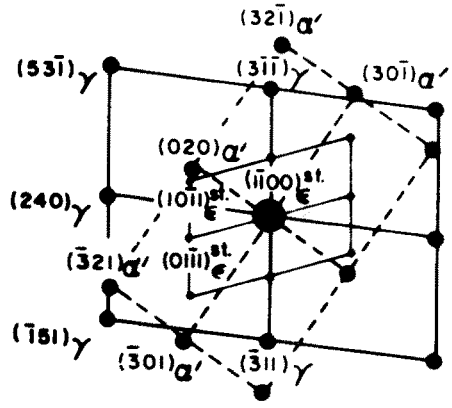

● - γ(fcc) austenite $[Z.A.]_\gamma = [2\bar{1}7]$

● - α′(bcc) martensite $[Z.A.]_{\alpha'} = [103]$

• - ε (hcp) martensite $[Z.A.]_\varepsilon = [\bar{1}\bar{1}23]$

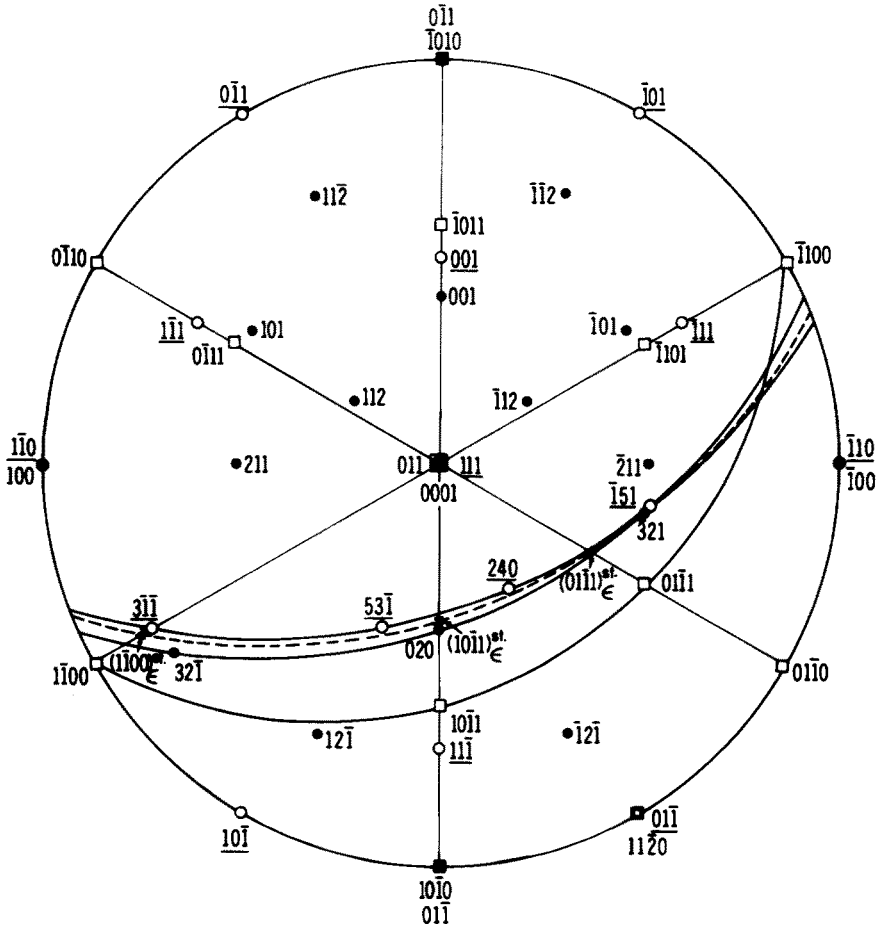

o - γ(fcc) phase

● - α′(bcc) phase

□ - ε (hcp) phase

--×-- Plane of diffraction pattern

γ(fcc)/ε(hcp)	γ(fcc)/α′(bcc)(NW)
$(\underline{111})\gamma \parallel (0002)\varepsilon$	$(\underline{111})\gamma \parallel (011)\alpha'$
$[0\underline{1}\bar{1}]\gamma \parallel [11\bar{2}0]\varepsilon$	$[1\bar{1}0]\gamma \parallel [100]\alpha'$

(c)

Figure 4 (a) Selected-area electron diffraction pattern of the Type 316 TiM stainless steel taken at the crack tip shown in Fig. 3. (b) Schematic diffraction pattern giving indices of reflections of γ-austenite, α′-martensite and the "streak spots" of ε-martensite. (c) Stereograms describing the analysis of the selected-area electron diffraction pattern represented in (a). (– – –) The constructed plane of the diffraction pattern.

the appearance of α'-martensite was found at the crack tip or within the grains after hydrogen charging and the crack propagated through the ε-phase and along the γ/ε interface [35].

In the light of the results described above, the 316 TiM stainless steel can be classified within the group of "unstable" stainless steels. Thus, the most striking result of these studies is the γ-phase instability induced by cathodic hydrogen charging of the annealed titanium-modified Type 316 stainless steel, because titanium additions are thought to improve the resistance of most stainless steels to the deleterious effects of hydrogen environments [4]. The formation of α'-martensite phase at the crack tip and in front of the crack, and the fact that upon further charging the crack propagated through the α'-phase, strongly suggest the tendency towards transgranular fracture under conditions of high hydrogen fugacities, as was reported for "unstable" stainless steels [5, 6, 36, 37]. The results further suggest that hydrogen which ingresses the specimen of "unstable" stainless steel that forms α'-martensite, can have the form of an autocatalytic process [38, 39]. Crack initiation occurs through triaxial stresses caused by hydrogen penetration and evidently followed by the formation of α'(bcc) martensitic phase when hydrogen emerges from the specimen. The lattice diffusivity of hydrogen in various bcc iron alloys at room temperature ranges toward from $10^{-8}\,cm^2\,sec^{-1}$ [40, 41] and is $\sim 10^{-12}\,cm^2\,sec^{-1}$ for the fcc phase [42]. Therefore, the existence of the bcc phase ahead of the advancing crack may simply provide a rapid diffusion path for hydrogen. In addition, hydrogen migrates to a region of high triaxial stress in front of the crack. Crack propagation will occur through the embrittled martensite phase which in turn aids in martensite formation.

4. Conclusions

1. Titanium addition to the solution-annealed and cathodically hydrogen charged Type 316 stainless steel was not found to increase the γ-phase stability.

2. The formation of α'-martensite phase ahead of the crack tip and in front of the crack and the fact that crack propagation occurred through the α'-phase, strongly suggests the tendency towards transgranular fracture under conditions of high hydrogen fugacities.

3. The α'-martensite phase was also found within the grains of Type 316 TiM stainless steel after hydrogen charging.

4. Crack propagation of "unstable" stainless steels that form α'-martensite, can have the form of an autocatalytic process.

References

1. M. B. WHITEMAN and A. R. TROIANO, *Corrosion* **21** (1965) 53.
2. M. R. LOUTHAN Jr, in "Hydrogen in Metals", edited by I. M. Bernstein and A. W. Thompson (ASM, Metals Park, Ohio, 1974) p. 53.
3. D. ELIEZER, D. G. CHAKRAPANI, C. J. ALTSETTER and E. N. PUGH, *Met. Trans. A* **10A** (1979) 935.
4. A. W. THOMPSON, in "Environment-sensitive Fracture of Engineering Materials", edited by Z. A. Foroulis (AIME, Warrendale, Pennsylvania, 1979) p. 379.
5. C. L. BRIANT, *Met. Trans. A.* **10A** (1979) 181.
6. E. MINKOVITZ and D. ELIEZER, *J. Mater. Sci.* **17** (1982) 3165.
7. *Idem, Scripta Metall.* **16** (1982) 981.
8. N. NARITA, C. J. ALTSTETTER and H. K. BIRNBAUM, *Met. Trans. A.* **13A** (1982) 1355.
9. A. P. BENTLEY and G. C. SMITH, *ibid.* **17A** (1986) 1593.
10. N. NARITA and H. K. BIRNBAUM, *Scripta Metall.* **14** (1980) 1355.
11. E. MINKOVITZ and D. ELIEZER, *J. Mater. Sci. Lett.* **1** (1982) 192.
12. E. MINKOVITZ, M. TALIANKER and D. ELIEZER, *J. Mater. Sci.* **16** (1981) 3506.
13. J. M. RIGSBEE, *Metallogr.* **11** (1978) 493.
14. D. ELIEZER, *J. Mater. Sci.* **18** (1983) 1540.
15. T. NAKAYAMA and M. TAKANO, *Corrosion* **38** (1982) 1.
16. M. L. HOLZWORTH and M. R. LOUTHAN Jr, *ibid.* **24** (1968) 110.
17. H. MATHIAS, Y. KATZ and S. NADIV, *Met. Sci.* **12** (1978) 129.
18. P. ROZENAK and D. ELIEZER, *Acta Metall.* **35** (1987) 2329.
19. K. KAMACHI, *Trans. ISIJ* **18** (1978) 485.
20. A. SZUMMER and A. JANKO, *Corrosion* **35** (1979) 461.
21. H. OKADA, Y. HOSOI and S. ABE, *ibid.* **26** (1970) 183.
22. R. LIU, N. NARITA, C. ALTSTETTER, H. BIRNBAUM and E. N. PUGH, *Met. Trans. A* **11A** (1982) 1563.
23. R. J. ASARO, A. J. WEST and W. A. TILLER, "Stress Corrosion Cracking and Hydrogen Embrittlement of Iron Base Alloys" (NACE, Houston, 1977) p. 1115.
24. E. E. BLOOM, J. M. LEITNAKER and J. O. STIEGLER, *Nucl. Technol.* **31** (1976) 232.
25. P. J. MAZIASZ, *Scripta Metall.* **14** (1980) 1251.
26. P. J. MAZIASZ and T. K. ROCHE, *J. Nucl. Mater.* **103/104** (1981) 797.
27. A. CHRISTENSEN, *J. Cryst. Growth* **33** (1976) 9.
28. BEATTLE and VER SNYDER, *Trans. ASM*, **45** (1953) 397.
29. KUDIELKA and RHODE, *Z. Krist.* **114** (1960) 447.
30. Z. NISHYIAMA, *Sci. Rep. Tokohu Univ.* **23** (1934) 638.
31. G. WASSERMAN, *Arch. Eisenhuttenw.* **16** (1983) 647.
32. E. MINKOVITZ, M. TALIANKER and D. ELIEZER, *Mater. Sci. Engng* **83** (1986) 269.
33. J. DASH and H. M. OTTE, *Acta Metall.* **11** (1963) 1169.
34. M. B. WHITEMAN and A. R. TROIANO, *Phys. Status Solidi* **7** (1964) K 109.
35. E. MANOR-MINKOVITZ and D. ELIEZER, *Scripta Metall.* **22** (1988) 1493.
36. H. HANNINEN and J. HAKARAINEN, *Corrosion* **36** (1980) 47.
37. D. ELIEZER, D. G. CHAKRAPANI, C. J. ALTSTETTER and E. N. PUGH, Proceedings of the Second International Congress on Hydrogen in Metals (Pergamon, New York, 1977) p. 3F5.
38. C. EDELEANU, "Stress-Corrosion Cracking and Embrittlement" (Wiley, New York, 1956) p. 126.
39. S. S. BIRLEY and D. TROMANS, *Corrosion* **27** (1971) 63.
40. K. W. LANGE and H. J. KONIG, "Proceedings of the Second International Conference on Hydrogen in Metals" (Pergamon, New York, 1977) p. 1A5.
41. Y. SAKAMOTO and U. HANADA, *ibid.* p. 1A7.
42. H. K. BIRNBAUM and C. A. WERT, *Ber. Bunsenges, Ges.* **76** (1972) 806.

Received 9 March
and accepted 27 July 1988